Hindawi Publishing Corporation
Mathematical Problems in Engineering
Volume 2012, Article ID 809187, 22 pages
doi:10.1155/2012/809187

Research Article

Adaptive Sliding Mode Control of Single-Phase Shunt Active Power Filter

Juntao Fei, Shenglei Zhang, and Jian Zhou

Jiangsu Key Laboratory of Power Transmission and Distribution Equipment Technology, College of Computer and Information, Hohai University, Changzhou 213022, China

Correspondence should be addressed to Juntao Fei, jtfei@yahoo.com

Received 22 August 2012; Revised 23 September 2012; Accepted 24 September 2012

Academic Editor: Piermarco Cannarsa

This paper presents a thorough study of the adaptive sliding mode technique with application to single-phase shunt active power filter (APF). Based on the basic principle of single-phase shunt APF, the approximate dynamic model is derived. A model reference adaptive sliding mode control algorithm is proposed to implement the harmonic compensation for the single-phase shunt APF. This method will use the tracking error of harmonic and APF current as the control input and adopt the tracking error of reference model and APF output as the control objects of adaptive sliding mode. In the reference current track loop, a novel adaptive sliding mode controller is implemented to tracking the reference currents, thus improving harmonic treating performance. Simulation results demonstrate the satisfactory control performance and rapid compensation ability of the proposed control approach under different conditions of the nonlinear load current distortion and the mutation load, respectively.

1. Introduction

With the widely used single-phase electric devices and increased high power electric appliance, it becomes more and more obvious that the quality of power supply drops and power factor reduces because of nonlinear factors. Since power electronic device and nonlinear load seriously damage the power quality, they have become the main harmonic pollution source of power network. APF could compensate the harmonics generated by the load current through injecting compensation current to the grid, having the advantages of high controllability and fast response. It not only can compensate harmonics, but also can inhibit the flicker and compensate reactive power; therefore, it is an effective approach to suppress the harmonic pollution.

In recent years, the research and design of APF have made great progress, and a large number of successful APF products have been put into market. Along with the rapid development of precision, the speed and reliability in hardware equipment, high performance algorithm, and real time control can be realized. The models of APF have been established using various methods, and the behavior of reference signal tracking has been improved using advanced control approaches. Rahmani et al. [1] presented a nonlinear control technique with experimental design for three-phase shunt APF. Singh et al. [2] designed a simple fuzzy logic-based robust APF to minimize the harmonics for wide range of variation of load current under stochastic conditions. Bhende et al. [3] proposed TS-fuzzy-controlled APF for load compensation. Montero et al. [4] compared some control strategies for shunt APFs in three-phase four-wire systems. Matas et al. [5] succeeded in linearizing the mathematical model of APF with feedback linearization method. Hua et al. [6] and Komucugil and Kukrer [7] used Lyapunov function to design some new control strategies for single-phase shunt APFs. Chang and Shee [8] proposed novel reference compensation current strategy for shunt APF control. Pereira et al. [9] derived new strategies with adaptive filters in APFs. Marconi et al. [10] proposed robust nonlinear control of shunt active filters for harmonic current compensation. APF control methods based on the adaptive algorithm have been proposed by some researchers [11–15]. Asiminoaei et al. [11] derived adaptive compensation scheme of reactive power for APF. Luo et al. [12] developed hybrid APF based on the adaptive fuzzy dividing frequency control method. Ribeiro et al. [13] presented a robust adaptive control strategy for power factor correction, harmonic compensation, and balancing of nonlinear loads in APFs. Valdez et al. [14] designed an adaptive controller for shunt active filter in the presence of a dynamic load and the line impedance. Shyu et al. [15] proposed a model reference adaptive controller to control the circuit and improve the current and reduce the current harmonics by using the approximate dynamic model of single phase shunt APF. Different control methods and harmonic suppression approaches for APF have been investigated [16, 17].

In the presence of model uncertainties and external disturbance, sliding mode control is necessary to incorporate into the adaptive control system since sliding mode control is a robust control technique which has many attractive features such as robustness to parameter variations and insensitivity to disturbance. Adaptive sliding mode control has the advantages of combining the robustness of variable structure methods with the tracking capability of adaptive control. However, systematic stability analysis and controller design of the adaptive sliding mode control with application to single-phase shunt APF have not been found in the literature; therefore, it is necessary to adopt adaptive sliding mode control that can on-line adjust the control parameter vector combined with the great robustness of sliding mode control for the harmonic suppression of single-phase shunt APF.

This paper will expand the model reference adaptive control (MRAC) and incorporate the sliding mode control into the adaptive system to design the adaptive sliding mode control algorithm and apply to the single-phase shunt APF. The contribution of this paper can be summarized as the following.

(1) A novel adaptive sliding mode control is proposed in reference current tracking to reduce the tracking error. The designed APF has superior harmonic treating performance and minimizes the harmonics for wide range of variation of load current under different nonlinear load; therefore, an improved THD performance can be achieved with the proposed control scheme.

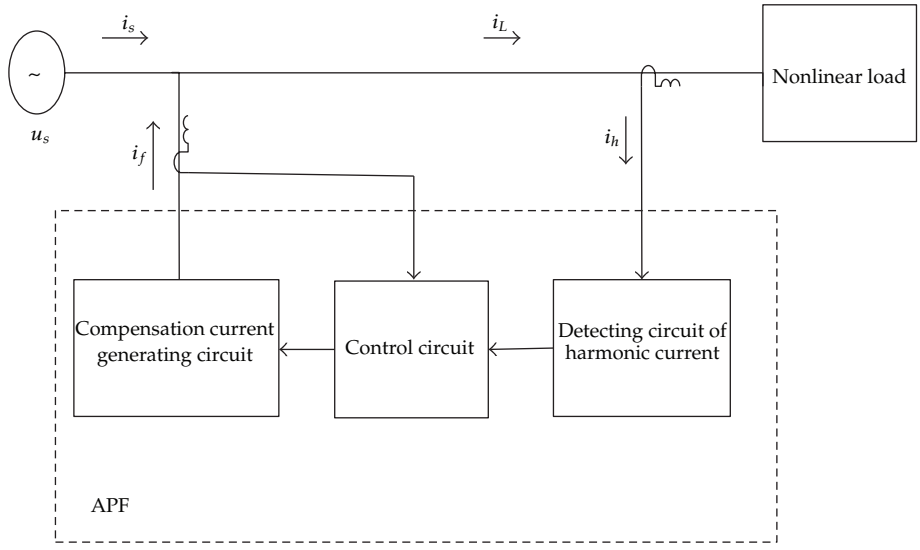

Figure 1: Principle diagram of SAPF.

(2) It is the first time that adaptive sliding mode control is applied to the APF. The advantage of using adaptive controller for the shunt APF with sliding mode technique is that it has better harmonic treating performance and will improve the robustness of the APF under the nonlinear loads.

(3) This paper systematically and deeply studies the adaptive control and sliding mode technique with application to APF, comprehensively uses the adaptive control, sliding mode control with the APF, thereby significantly reducing the APF's sensitivity to the nonlinear load and disturbance, and improving the robust performance. The APF control system is designed to make the compensation current track the command signal in real time, thereby eliminating the harmonics, improving the electric energy quality, and enhancing the security of the power transmission and distribution and power grid. Therefore, this research has great theoretical value and application potentials.

The paper is organized as follows. In Section 2, the basic principle of single-phase shunt APF and the approximate dynamic model are introduced. In Section 3, an adaptive sliding mode controller for shunt APF is designed and Lyapunov stability is established. Simulation results are presented in Section 4. Concluding remarks are summarized in Section 5.

2. Dynamic Model of APF

In this section, the basic principle of single-phase shunt APF and the approximate dynamic model are introduced [15]. Main circuit of shunt APF in parallel with the load connected to the network is shown in Figure 1. Currently, this is the most basic form of APF and the most widely used. In this way, the APF is equivalent to current generator, and the current value is the compensation current.

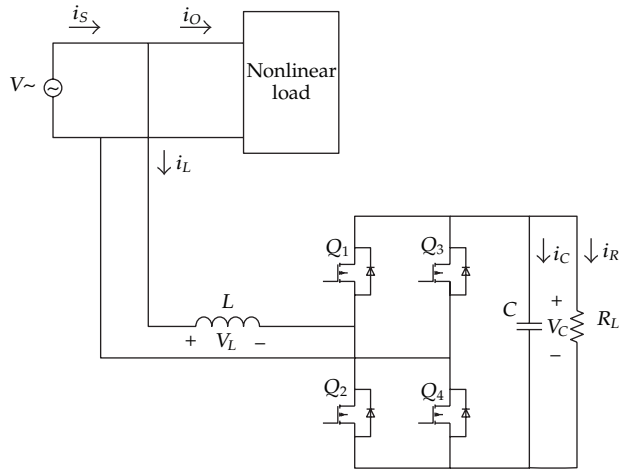

Figure 2: Single phase SAPF and nonlinear loads in parallel.

As shown in Figure 2, APF connected in parallel with the load could cancel the harmonic components in the line current (i_S) so that the current flowing into and from the power line is sinusoidal and in phase with the power line voltage. In other words, the compensating current (i_L) is injected into the line to force the line current (i_S) to become sinusoidal wave and to achieve a unity power factor.

The current of the shunt APF can be expressed as

$$i_S = i_O + i_L, \tag{2.1}$$

where i_O is the nonlinear load current.

The operation of the APF can be divided into two modes, and its four switches have a switching frequency of f_S. In mode 1, Q_2 and Q_3 are turned ON, while Q_1 and Q_4 are turned OFF when $0 < t < DT_S$, where $T_S = 1/f_S$ is the switching period and $D = T_{\mathrm{ON}}/T_S$ is the duty ratio. In mode 2, the switching states of four switches in mode 1 are reversed when $DT_S < t < T_S$.

By observing the equivalent circuits that are shown in Figure 3, one circuit shows the inductor voltage and current during one switching cycle when $v_S > 0$, which are expressed by the following:

$$\begin{aligned} v_L(t) &= v_S + v_C \\ i_L(t) &= i_L(0) + \frac{1}{L}\int_0^{DT_S} (v_S + v_C)dt \quad \text{for } 0 \le t \le DT_S, \\ v_L(t) &= v_S - v_C \\ i_L(t) &= i_L(DT_S) + \frac{1}{L}\int_{DT_S}^{T_S} (v_S - v_C)dt \quad \text{for } DT_S \le t \le T_S. \end{aligned} \tag{2.2}$$

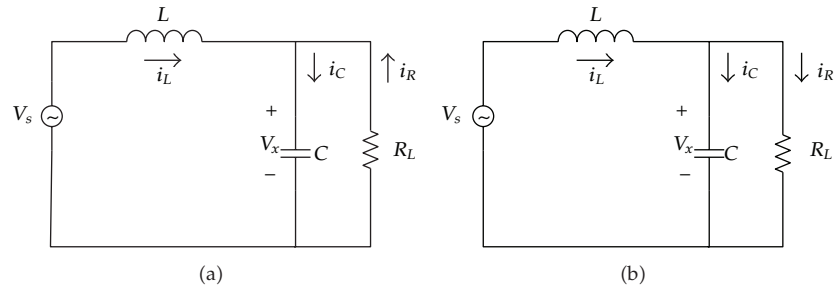

Figure 3: Equivalent circuit of APF (a) equivalent circuit when $0 < t < DT_S$ and (b) equivalent circuit when $DT_S < t < T_S$.

Figures 3(a) and 3(b) show the equivalent circuits at one switching cycle. Define the switching function S_n of each switch as

$$S_n = \begin{cases} 1 & \text{when } Q_n \text{ is turned ON,} \\ 0 & \text{when } Q_n \text{ is turned OFF,} \end{cases} \tag{2.3}$$

where $n = 1-4$ is denoted as the switch number.

Therefore, the state equations of the inductor current and the capacitor voltage are written by Kirchhoff's laws

$$\begin{aligned} \dot{i_L} &= \frac{1}{L}[v_S - Sv_C], \\ \dot{v_C} &= \frac{1}{C}\left[Si_L - \frac{v_C}{R_L}\right], \end{aligned} \tag{2.4}$$

where $S = (S_1 - S_2)$. In the following expressions, $x_1(t)$ and $x_2(t)$ represent the state variables of the average values of the inductor current and the capacitor voltage over a switching period, respectively. Substituting $S = 1$ and $S = -1$ into (2.4) yields

$$\begin{aligned} x_1(t) &= \frac{1}{T_S}\int_t^{t+T_S} i_L(\tau)d\tau, \\ x_2(t) &= \frac{1}{T_S}\int_t^{t+T_S} v_C(\tau)d\tau. \end{aligned} \tag{2.5}$$

The average state-space model of the converter can be written as

$$\begin{aligned} \frac{dx_1}{dt} &= \left(\frac{v_S + v_C}{L}\right)u + \left(\frac{v_S - v_C}{L}\right)(1-u), \\ \frac{dx_2}{dt} &= \left(\frac{-i_L}{C} - \frac{v_C}{R_L C}\right)u + \left(\frac{i_L}{C} - \frac{v_C}{R_L C}\right)(1-u), \end{aligned} \tag{2.6}$$

where u is the duty ratio, which can take any value between 0 and 1. Rearranging (2.6) yields

$$\begin{aligned}\frac{dx_1}{dt} &= \frac{(2u-1)x_2}{L} + \frac{v_S}{L},\\ \frac{dx_2}{dt} &= \frac{(1-2u)x_1}{C} - \frac{x_2}{R_L C}.\end{aligned} \tag{2.7}$$

Consequently, the dynamic behavior of the APF can be described by the following state-space model:

$$\dot{x} = Fx + Gxu + Ew, \tag{2.8}$$

where

$$x = \begin{bmatrix} i_L & v_C \end{bmatrix}^T, \quad F = \begin{bmatrix} 0 & \frac{-1}{L} \\ \frac{1}{C} & \frac{-1}{R_L C} \end{bmatrix}, \quad G = \begin{bmatrix} 0 & \frac{2}{L} \\ \frac{-2}{C} & 0 \end{bmatrix}, \quad E = \begin{bmatrix} \frac{1}{L} & 0 \end{bmatrix}^T. \quad w = v_S, \tag{2.9}$$

Now, consider the bilinear state equation (2.8). If $x = x_0$ and $u = u_0$ suffice to

$$f(x_0, u_0) = Fx_0 + Gx_0u_0 + Ew(t) = 0, \tag{2.10}$$

(x_0, u_0) is called its equilibrium or operating point. Let

$$0 = f(x_0, u_0, w, t) = Fx_0 + Gx_0u_0 + Ew(t). \tag{2.11}$$

We can expand the right-hand side of (2.11) into a Taylor series about (x_0, u_0) and then neglect the high-order terms so that

$$\dot{x} = f(x_0, u_0) + \left.\frac{\partial f}{\partial x}\right|_{\substack{x=x_0\\u=u_0}} (x - x_0) + \left.\frac{\partial f}{\partial u}\right|_{\substack{x=x_0\\u=u_0}} (u - u_0). \tag{2.12}$$

Moreover, since our interest is on the trajectories near (x_0, u_0), let $x_\delta = x - x_0$, $u_\delta = u - u_0$, and we have the following:

$$\dot{x}_\delta = (F + Gu_0)x_\delta + (Gx_0)u_\delta \equiv A_p x_\delta + B_p\ u_\delta, \tag{2.13}$$

where $A_p = F + Gu_0$ and $B_p = Gx_0$.

The bilinear state equation (2.10) can be approximately described by a linear state equation of the form (2.13).

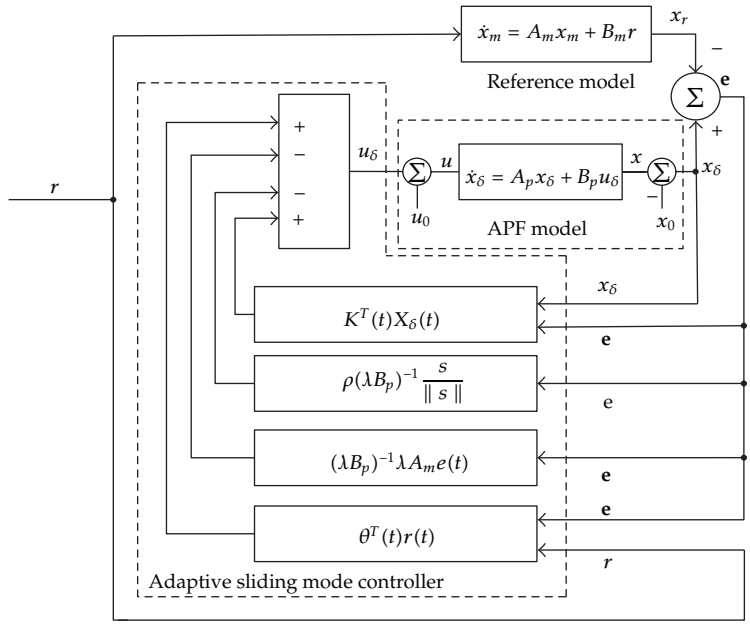

Figure 4: block diagram of adaptive sliding mode control approach.

Considering the equilibrium of bilinear state equation (2.13), the equilibrium values of the inductor current and the capacitor voltage can be obtained as

$$\begin{aligned} x_{02} &= \frac{v_S}{1-2u_0}, \\ x_{01} &= \frac{x_{02}}{R_L(1-2u_0)}, \end{aligned} \tag{2.14}$$

where x_{02} and x_{01} are the equilibrium values of v_C and i_L, respectively. The average value of the duty ratio u_0 can be obtained from (2.15) as

$$u_0 = \frac{1}{2}\left(1 - \frac{v_S}{x_{02}}\right). \tag{2.15}$$

It should be noted that by setting the DC voltage and controlling the duty ratio, we could control the inductor current, and thus the APF can work.

3. Design of Adaptive Sliding Mode Controller

In this section, a detailed study of the shunt APF with parameter uncertainties is proposed. A new adaptive sliding mode control strategy for shunt APF using a proportional sliding surface is proposed, and an adaptive sliding law to overcome the parameter uncertainties is also derived. The block diagram of the designed adaptive sliding mode controller for APF is shown in Figure 4.

The goal of APF control is to design an adaptive sliding mode controller so that the APF output trajectory can track the reference model.

Rewriting the linear state equation (2.13), we will obtain the following:

$$\dot{X}_\delta = A_P X_\delta + B_P u_\delta. \tag{3.1}$$

Consider the system (3.1) with parametric uncertainties, that is, the linearization errors such as high-order terms in Taylor series (2.12),

$$\dot{X}_\delta = (A_P + \Delta A_P)X_\delta(t) + (B_P + \Delta B_P)u_\delta + f_d, \tag{3.2}$$

where ΔA_P is the unknown parameter uncertainties of the matrix A_P, ΔB_P is the unknown parameter uncertainties of the matrix B_P, and f_d is external disturbances such as nonlinear loads in the APF.

The reference model is defined as

$$\dot{X}_m = A_m X_m + B_m r, \tag{3.3}$$

where A_m, B_m are known constant matrices of a reference model and r is reference input.

We make the following assumptions.

Assumption 3.1. There exist unknown matrices of appropriate dimensions D, G such that $\Delta A_P(t) = B_P D(t) + \Delta \widetilde{A}_P(t)$, $\Delta B_P(t) = B_P G(t) + \Delta \widetilde{B}_P(t)$, where $B_P D(t)$ and $B_P G(t)$ are matched uncertainty, $\Delta \widetilde{A}_P(t)$ and $\Delta \widetilde{B}_P(t)$ are unmatched uncertainty. From this assumptions, (3.2) can be rewritten as

$$\dot{X}_\delta = A_P X_\delta(t) + B_P u_\delta + B_P f_m + f_u, \tag{3.4}$$

where $f_m(t, X_\delta, u_\delta)$ represents the matched lumped uncertainty and $f_u(t, X_\delta, u_\delta)$ represents the unmatched lumped uncertainty, respectively, which is given by

$$\begin{aligned} f_m(t, X_\delta, u_\delta) &= D(t)X_\delta(t) + G(t)u_\delta, \\ f_u(t, X_\delta, u_\delta) &= \Delta \widetilde{A}_P(t)X_\delta(t) + \Delta \widetilde{B}_P(t)u_\delta. \end{aligned} \tag{3.5}$$

Assumption 3.2. The matched and unmatched lumped uncertainty f_m and f_u are bounded such as $\|f_m(t, X_\delta, u_\delta)\| \leq \alpha_m$ and $\|f_u(t, X_\delta, u_\delta)\| \leq \alpha_u$, where α_m, α_u are known positive constants.

Assumption 3.3. There exist constant matrices K^* and θ^* such that the following matching conditions $A_P + B_P K^{*T} = A_m$ and $B_P \theta^{*T} = B_m$ can always be satisfied.

Then, the adaptive sliding mode controller will be designed.

The tracking error and its derivative are

$$\begin{aligned} e &= X_\delta - X_m, \\ \dot{e} &= A_m e + (A_P - A_m)X_\delta + B_P u_\delta - B_m r + B_P f_m + f_u. \end{aligned} \tag{3.6}$$

The proportional sliding surface is defined as

$$s(t) = \lambda e, \tag{3.7}$$

where λ is a constant matrix satisfying that λB_P is a nonsingular diagonal matrix.

The derivative of the sliding surface is

$$\dot{s} = \lambda \dot{e} = \lambda A_m e + \lambda(A_P - A_m)X_\delta + \lambda B_P u_\delta - \lambda B_m r + \lambda B_P f_m + \lambda f_u. \tag{3.8}$$

Setting $\dot{s} = 0$ to solve equivalent control u_{eq} gives

$$u_{eq} = -(\lambda B_P)^{-1}\lambda A_m e - (\lambda B_P)^{-1}\lambda(A_P - A_m)X_\delta + (\lambda B_P)^{-1}\lambda B_m r - f_m - (\lambda B_P)^{-1}\lambda f. \tag{3.9}$$

From Assumption 3.3 and (3.9) can be rewritten as

$$u_{eq} = -(\lambda B_P)^{-1}\lambda A_m e + K^{*T}X_\delta + \theta^{*T} r - f_m - (\lambda B_P)^{-1}\lambda f. \tag{3.10}$$

Since the equivalent control u_{eq} (3.10) gives the controller structure of what we should propose and the unknown disturbance term f_m and f_u can be dealt with the sliding mode terms, the control signal u_δ can be proposed as

$$u_\delta = -(\lambda B_P)^{-1}\lambda A_m e + K^{*T}X_\delta + \theta^{*T} r - \rho(\lambda B_P)^{-1}\frac{s}{\|s\|}, \tag{3.11}$$

where ρ is constant, $s/\|s\|$ is the sliding mode unit control signal.

The adaptive sliding mode version of control input is

$$u_\delta(t) = -(\lambda B_P)^{-1}\lambda A_m e(t) + K^T(t)X_\delta(t) + \theta^T(t) r(t) - \rho(\lambda B_P)^{-1}\frac{s}{\|s\|}, \tag{3.12}$$

where $K(t)$ is the estimate of K^*, $\theta(t)$ is the estimate of θ^*.

Define the estimation error as

$$\begin{aligned} \widetilde{K}(t) &= K(t) - K^*, \\ \widetilde{\theta}(t) &= \theta(t) - \theta^*. \end{aligned} \tag{3.13}$$

Substituting (3.13) into (3.12) yields

$$u_\delta(t) = -(\lambda B_P)^{-1}\lambda A_m e(t) + \left[\widetilde{K}^T(t) + K^{*T}\right]X_\delta(t) + \left[\widetilde{\theta}^T(t) + \theta^{*T}\right]r(t) - \rho(\lambda B_P)^{-1}\frac{s}{\|s\|}. \quad (3.14)$$

From (3.14) and Assumption 3.3, rewrite (3.3) as follows

$$\begin{aligned}\dot{X}_\delta(t) = & -B_P(\lambda B_P)^1\lambda A_m e(t) + B_P\widetilde{K}^T(t)X_\delta(t) + A_m X_\delta(t) \\ & + B_P\widetilde{\theta}^T(t)r(t) + B_m r(t) - B_P\rho(\lambda B_P)^{-1}\frac{s}{\|s\|} + B_P f_m + f_u.\end{aligned} \quad (3.15)$$

Then, we have the derivative of the tracking error equation:

$$\begin{aligned}\dot{e}(t) = & -B_P(\lambda B_P)^{-1}\lambda A_m e(t) + B_P\widetilde{K}^T(t)X_\delta(t) + B_P\widetilde{\theta}^T(t)r(t) + A_m e(t) - B_P\rho(\lambda B_P)^{-1}\frac{s}{\|s\|} \\ & + B_P f_m + f_u \\ = & \left[I - B_P(\lambda B_P)^{-1}\lambda\right]A_m e(t) + B_P\widetilde{K}^T(t)X_\delta(t) + B_P\widetilde{\theta}^T(t)r(t) - B_P\rho(\lambda B_P)^{-1}\frac{s}{\|s\|} + B_P f_m + f_u,\end{aligned} \quad (3.16)$$

and the derivative of $s(t)$ is

$$\dot{s}(t) = \lambda B_P\widetilde{K}^T(t)X_\delta(t) + \lambda B_P\widetilde{\theta}^T(t)r(t) - \rho\frac{s}{\|s\|} + \lambda B_P f_m + \lambda f_u. \quad (3.17)$$

Define a Lyapunov function

$$V = \frac{1}{2}s^T s + \frac{1}{2}\operatorname{tr}\left[\widetilde{K}M^{-1}\widetilde{K}^T\right] + \frac{1}{2}\operatorname{tr}\left[\widetilde{\theta}N^{-1}\widetilde{\theta}^T\right], \quad (3.18)$$

where M, N are positive definite matrix, tr denoting the trace of a square matrix.

Differentiating V with respect to time yields

$$\begin{aligned}\dot{V} = & s^T\dot{s} + \operatorname{tr}\left[\widetilde{K}M^{-1}\dot{\widetilde{K}}^T\right] + \operatorname{tr}\left[\widetilde{\theta}N^{-1}\dot{\widetilde{\theta}}^T\right] \\ = & -\rho\|s\| + s^T\lambda B_P f_m + s^T\lambda f_u + s^T\lambda B_P\widetilde{K}^T(t)X_\delta(t) + \operatorname{tr}\left[\widetilde{K}M^{-1}\dot{\widetilde{K}}^T\right] \\ & + s^T\lambda B_P\widetilde{\theta}^T(t)r(t) + \operatorname{tr}\left[\widetilde{\theta}N^{-1}\dot{\widetilde{\theta}}^T\right].\end{aligned} \quad (3.19)$$

For $s^T\lambda B_P\widetilde{K}^T(t)X_\delta(t)$ and $s^T\lambda B_P\widetilde{\theta}^T(t)r(t)$ are scalar, from the properties of matrix trace $x^TAx = \mathrm{tr}(xx^TA)$, $\mathrm{tr}(A) = \mathrm{tr}(A^T)$ there have

$$\begin{aligned} s^T\lambda B_P\widetilde{K}^T(t)X_\delta(t) &= \mathrm{tr}\left[X_\delta(t)s^T\lambda B_P\widetilde{K}^T(t)\right] = \mathrm{tr}\left[\widetilde{K}(t)B_P{}^T\lambda^T sX_\delta{}^T(t)\right], \\ s^T\lambda B_P\widetilde{\theta}^T(t)r(t) &= \mathrm{tr}\left[r(t)s^T\lambda B_P\widetilde{\theta}^T(t)\right] = \mathrm{tr}\left[\widetilde{\theta}(t)B_P{}^T\lambda^T sr^T(t)\right]. \end{aligned} \tag{3.20}$$

To make $\dot{V} \le 0$, we choose the adaptive laws as

$$\begin{aligned} \dot{\widetilde{K}}^T(t) &= \dot{K}^T(t) = -MB_P{}^T\lambda^T sX_\delta{}^T(t), \\ \dot{\widetilde{\theta}}^T(t) &= \dot{\theta}^T(t) = -NB_P{}^T\lambda^T sr^T(t). \end{aligned} \tag{3.21}$$

This adaptive sliding law yields

$$\begin{aligned} \dot{V} =& -\rho\|s\| + s^T\lambda B_P f_m + s^T\lambda f_u \le -\rho\|s\| + \|s\|\|\lambda B_P\|\left\|f_m\right\| + \|s\|\|\lambda\|\left\|f_u\right\| \\ \le& -\rho\|s\| + \|s\|\|\lambda B_P\|\alpha_m + \|s\|\|\lambda\|\alpha_u \le -\|s\|\left(\rho - \|\lambda B_P\|\alpha_m - \|\lambda\|\alpha_u\right) \le 0, \end{aligned} \tag{3.22}$$

with $\rho \ge \|\lambda B_P\|\alpha_m + \|\lambda\|\alpha_u + \eta$, where η is a positive constant and $\dot{V}$ becomes negative semi-definite, that is, $\dot{V} \le -\eta\|s\|$. According to Barbalat's lemma [18], it can be proved that $s(t)$ will asymptotically converge to zero, $\lim_{t\to\infty}s(t) = 0$. Consequently, $e(t)$ will asymptotically converge to zero, $\lim_{t\to\infty}e(t) = 0$.

4. Simulation Analysis

In this section, the single-phase shunt APF using adaptive sliding mode control is implemented with MATLAB/SIMPOWER Toolbox. The goal of adaptive sliding mode control is to make the APF output current track the detected harmonic current. Simulations on APF system will verify the control effects of the proposed adaptive sliding approach.

First of all, the nonlinear load of simulation model is described. Nonlinear load: a load branch is rectifier bridge connecting parallel RC load, $R = 15\,\Omega$, $C = 5e-3F$. When 0–0.4 s, a load works, the total harmonic distortion (THD) of nonlinear load current is 45.82%; When 0.4–0.8 s, the breaker is switched on and another load branch which is the same as first one is injected, accompanied by a disturbance load (interference frequency $f = 1000\,\mathrm{Hz}$, square wave $T = 0.001\,\mathrm{s}$, pulse width 50%, parallel disturbance load $L = 0.2\,\mathrm{H}$, and $R = 20\,\Omega$), and the total harmonic distortion (THD) of nonlinear load current is 40.12%. The current mainly contains 3rd and 7th times, odd harmonic. The parameters of the proposed adaptive sliding mode controller are chosen as follows: $A_M = [-49.6\ -351.8;\ 519\ 0.21]$, $B_M = [7400;\ -8.6]$, $C_M = [1\ 0;\ 0\ 1]$, $D_M = [0;\ 0]$, $M = 5e-7$, $N = 5e-5$, $\rho = 200$, and $\lambda = [0.04\ 0.05]$. As DC voltage $V_C = 600\,\mathrm{V}$, it can be calculated that $x_0 = [0.11573;\ 600]$, $u_0 = 0.24077$. According to the APF circuit model, it is calculated that $A_p = [0\ -86.4;\ 518.5\ -0.1]$, $B_p = [200000;\ -231.5]$.

Because the rectifier bridge and nonlinear load result in harmonic and reactive currents, serious distortions of the circuit current show up. Figure 5 draws the current

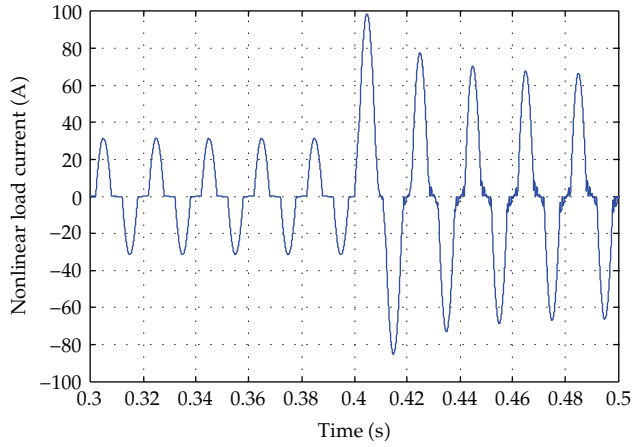

Figure 5: Nonlinear load current (before and after load change).

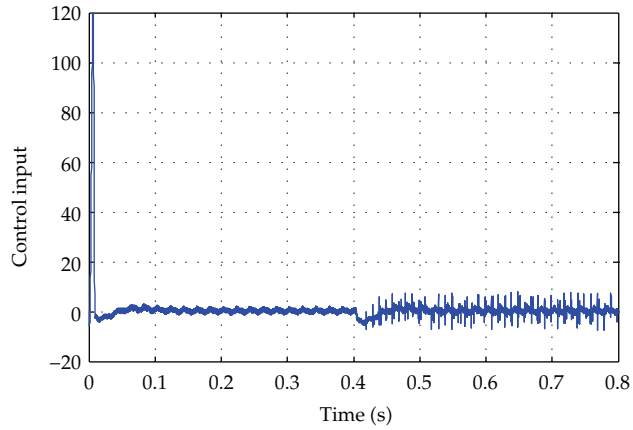

Figure 6: Input of adaptive sliding mode controller.

waveform before and after the nonlinear load change. Mutation distortions of current have serious effects on the power system and other electrical equipments that should be compensated and eliminated.

From the adaptive harmonic detection output i_h and the APF current i_L obtained from measuring module, we can get the input signal of adaptive sliding mode controller (which is also the reference model input signal) $r = i_h - i_L + i_{\mathrm{PI}}$, where i_{PI} is the compensation current of voltage PI control for APF DC side. Single-phase harmonic detection method is used, where the input has only sine wave signal, implying that the detection result i_h contains the harmonic and reactive current.

According to the approximation process of APF dynamic model, near the equilibrium point (x_0, u_0), the simulation variables $x_\delta = x - x_0$, $u_\delta = u - u_0$, so we can get x_δ, u from $x_\delta = x - x_0$, $u = u_\delta + u_0$, respectively.

The input waveform of adaptive sliding mode controller (i.e., input waveform of the reference model) is drawn in Figure 6. The controller not only can compensate and eliminate

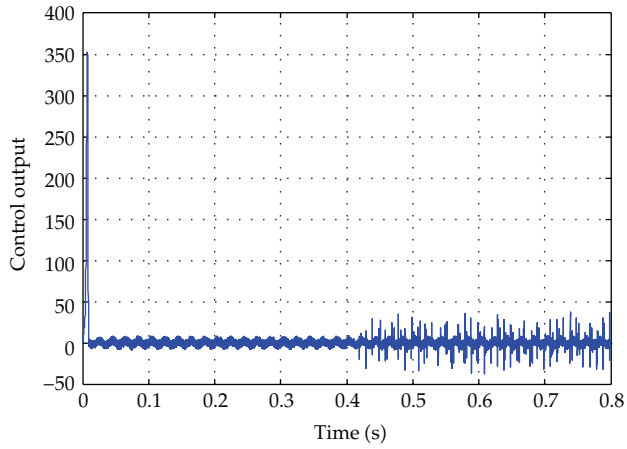

Figure 7: Output of adaptive sliding mode controller.

the harmonic, but also can compensate the DC voltage and make it stay stable in /near a predetermined value to improve the compensation effect.

The output of the adaptive sliding mode controller is shown in Figure 7. The output u of the controller compares with triangular waves which have similar amplitude with u, then PWM generator output is the standard of four-phase control pulse and can fully reflect the control function of controller output to the APF. PWM signal is generated using triangular wave comparison method, where the triangular wave amplitude is ±1 and frequency is 1000 Hz.

By controlling on or off of the four thyristors in the full-controlled bridge, four phase PWM pulse control signal will control the charging and discharging process of the DC side capacitor C, thereby producing the inductor current i_L, that is, APF compensating current. The parameters of APF main circuit: $L = 0.006$ H inductor, capacitor $C = 0.001$ F, $R = 10$ KΩ, thyristors using the IGBT/Diode module, a default parameter.

Figure 8 compares between the harmonic and APF current, where the red curve represents APF output current (inductor current) and blue curve represents detected harmonic current. Compared with the detected harmonic current, the APF output current has equal amplitude but opposite direction. The APF output current is injected into the nonlinear load current, then the harmonics and reactive current caused by nonlinear loads can be eliminated, thus the harmonic current compensation can be achieved. After 0.4 s, the load and interference are increased, and the APF current still can quickly track the harmonic current although there may have some errors between harmonic current and the APF output current even if the APF works stable. The errors mainly contain compensation current from PI control circuit of the DC voltage for the DC voltage compensation of APF.

Simulation of the PI control signal is shown in Figure 9. The initial moment due to the DC voltage is zero, and the output of PI controller is a big compensation signal, so that the DC voltage can quickly arrive at the setting value. After 0.4 s, the load and interference are increased, the harmonic is increased, and the DC voltage is reduced; the PI control output could adjust in time, then quickly recover normal working state.

Figure 10 shows that, after the circuit starts to work, the APF capacitor voltage quickly rises to more than 500 V and basically stays at a setting value near 600 V, rapidly adjusted by

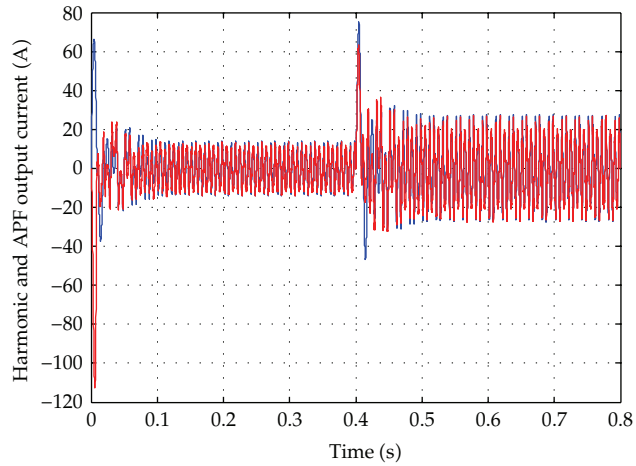

Figure 8: Harmonic and APF current.

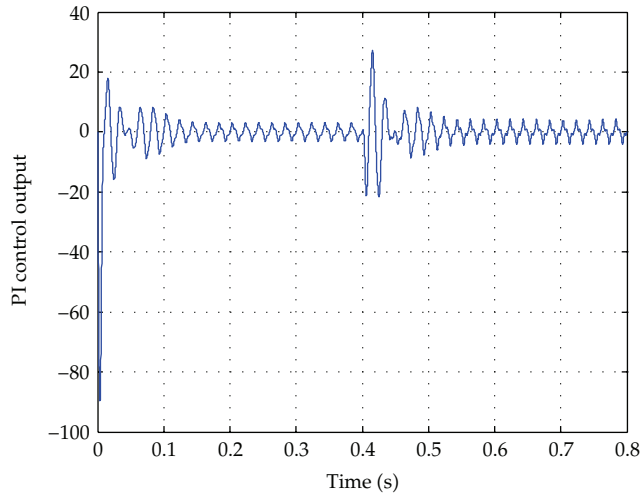

Figure 9: Output of DC voltage PI control.

the PI control of DC voltage. The load changed at 0.4 s, and the DC voltage could be quickly stabilized to the set value also.

Figure 10 plots the power current after APF has been compensated, where the Figure 11(b) zooms in on 0.4 s when the loads change. It can be seen from Figure 11 that the current waveform has been improved and adjusted rapidly to approximate standard sine wave within 0.08 s after the circuit started to work and load changed. Compared with the nonlinear load current waveform in Figure 5, it can be seen that before compensation the load current has serious distortion and after compensation the current quality has been obviously improved. Thus, the proposed purposes of nonlinear load current compensation through APF can be successfully achieved.

Through the FFT Analysis tools of SIMLINK powergui module, the load current and the power current are acquired.

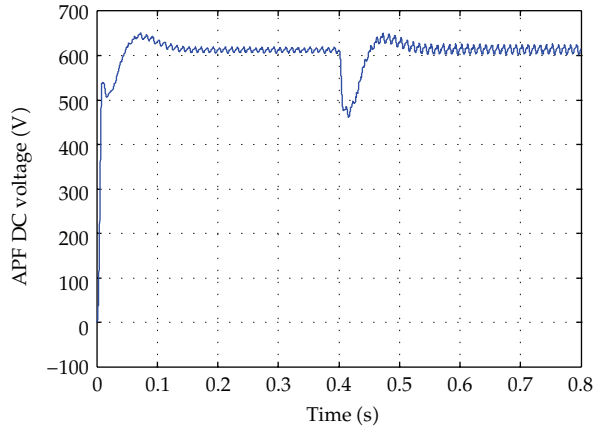

Figure 10: APF DC voltage.

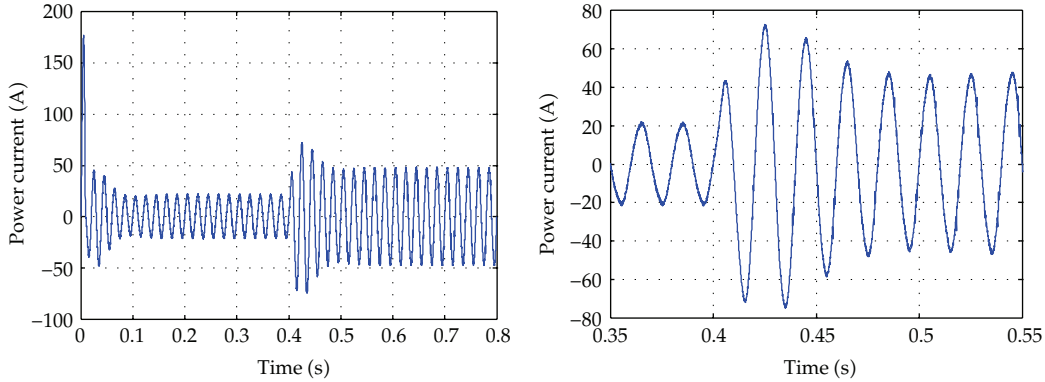

Figure 11: (a) Power current (0–0.8 s). (b) Power current (0.35–0.55 s) (nonlinear load changes in 0.4 seconds).

Figure 12 is the nonlinear load current waveform and its harmonic analysis. The serious waveform distortions can be observed. FFT analysis shows that nonlinear harmonic current is mainly 3rd and 7th harmonic interference and with a certain degree of 5th and higher harmonic interference. Power current waveform after APF is shown in Figure 13. After compensation, the 3rd harmonic is greatly reduced, the 7th harmonic is almost eliminated, all other higher harmonics are reduced, and the power current is approximate to sine wave. The compensated current THD is 3.5%, more than the national standard level of 5%. After load changed, nonlinear load current THD changed from 45.81% to 40.12% this is due to the percentage of nonlinear part load (bridge, capacitance, and inductance) relative to the linear portion (resistance) decreased. But we can still see the obvious distortion of nonlinear load current.

Figure 14 shows the current after load changed, the same bridge and nonlinear load (with certain high frequency interference) paralleled in the circuit. It can be seen that although the nonlinear load and the load current increase, the current waveform distortion is relatively minor as of 40.12% THD. The current waveform after APF compensation is

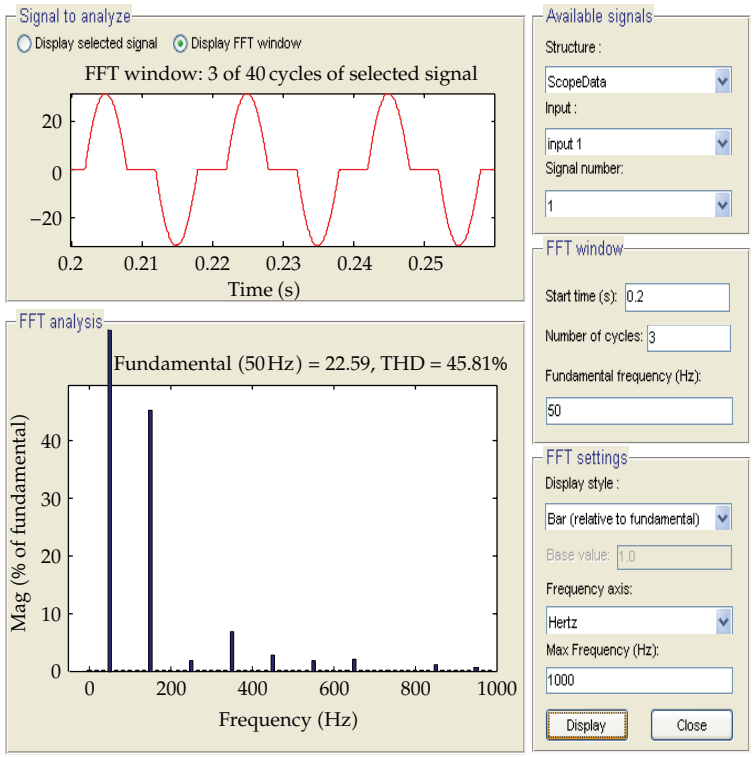

Figure 12: Nonlinear load current analysis (before load change).

shown in Figure 15. After compensation, the quality of power current is greatly improved with THD reaching at 3.28%; it demonstrates good compensation capability of APF using adaptive sliding mode controller. Because of the increase of load disturbance and the changes of currents, the compensated current has some minor glitches, but the power current quality remains within the national standard.

The control parameters K, e in the adaptive sliding mode controller are analyzed in the following steps. From Figures 16 and 17, it can be seen that the parameters can be adjusted to a stable value soon and the stability of the control system can be maintained, and the parameters K and θ can converge to constant and stay in stable state within 0.1 s, that is, within 4-5 circuit cycles.

The current error between model reference current item and APF inductance current and the voltage error between model reference voltage item and APF DC voltage are drawn in Figures 18 and 19, respectively. The tracking error $e = [\, e_i \; e_u \,]^T$ as parameters of adjustment process exist within the adaptive sliding mode process. It will decrease in a certain way and maintain in a certain range finally. The simulation is based on the actual APF model with nonlinear load and model uncertainties. Because of the complexity of the circuits and the approximation of the APF model, the parameters of APF model have some uncertainties. The tracking error can be quickly adjusted to dozens of magnitude of dimensionless parameters and to be maintained in a certain range.

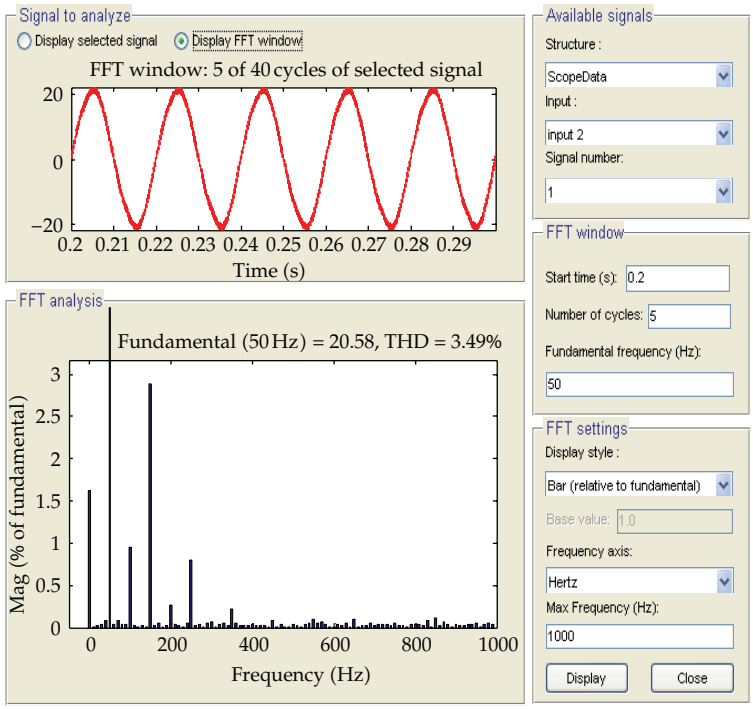

Figure 13: Power current after APF compensation (before load changes).

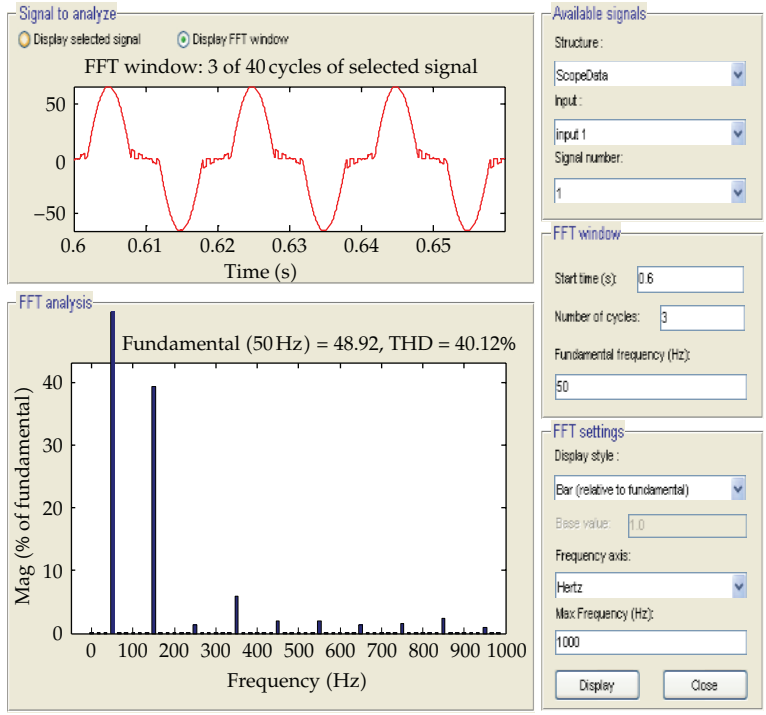

Figure 14: Nonlinear load current (after load change).

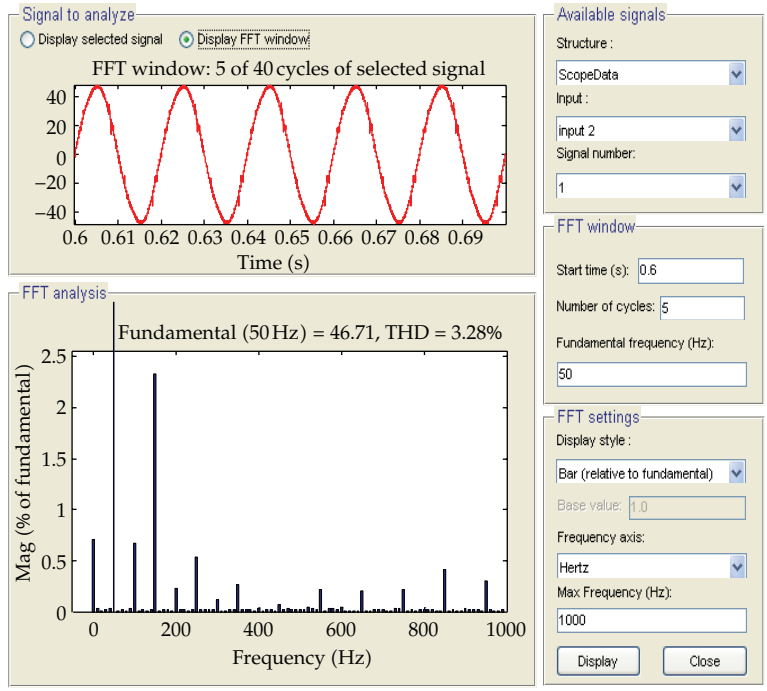

Figure 15: Power Current after APF Compensation (after load changes).

Table 1: Comparison of THD after compensation.

Controller type	Current type	Time period/THD of current	
		0–0.4 s	0.4–0.8 s
Without controller	Nonlinear load current	45.81%	40.12%
Adaptive controller	Power current after compensation	4.16%	3.54%
Adaptive sliding mode controller		3.49%	3.29%

It can be observed from Figures 20 and 21 that adaptive sliding mode control has better harmonic compensation performance that adaptive control, the index of THD, has been reduced with the adaptive sliding control.

Compared the waveforms before and after APF works, it can be seen from Table 1 that the adaptive sliding mode control not only has good compensation effect, but also has quick compensation ability. At the same time, the controller could optimize the adaptive parameters to make it more reasonable and make it possible for the investigation of the intelligent control. Simulation and analysis verified the feasibility of adaptive sliding mode control theory and showed good control effect in single-phase SAPF application.

5. Conclusion

This paper studied the principle and dynamic model of single-phase shunt APF and proposed a new adaptive sliding mode control algorithm. The simulation results proved that for nonlinear load current the adaptive sliding mode controller has successful compensation

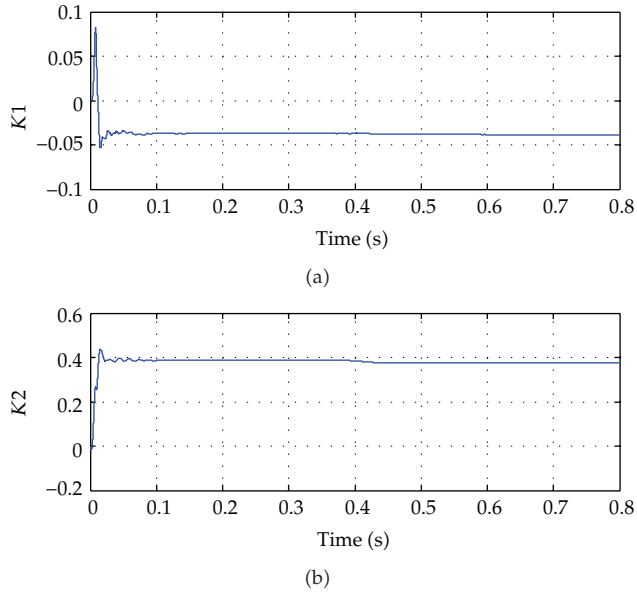

Figure 16: Controller parameters K.

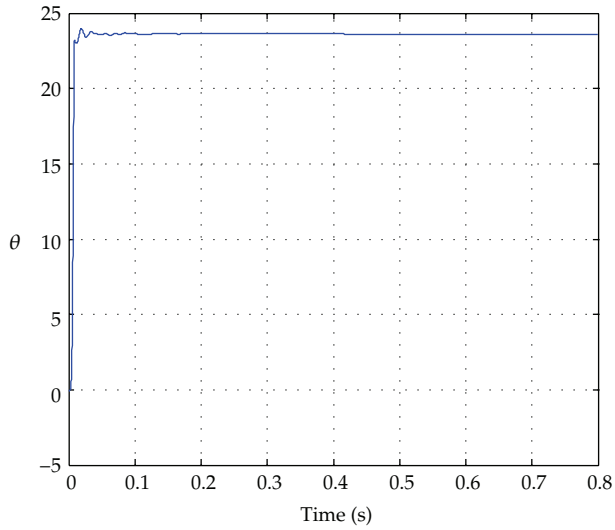

Figure 17: Controller parameter theta.

effect; that is, it can compensate the most harmonic current and eliminate certain reactive current, which can recover sine wave from severely detuned current waveform and improve the power factor. From Figure 9, we can see that the APF current can quickly track the harmonic current, thus to achieve the harmonic compensation. The reference currents tracking behavior has been improved, and the power supply harmonic current has been reduced with novel adaptive sliding mode control. The proposed control system has the

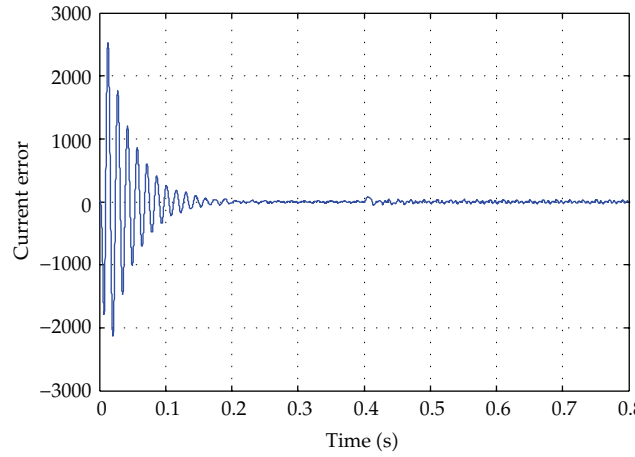

Figure 18: Current error between model reference current item and APF inductance current.

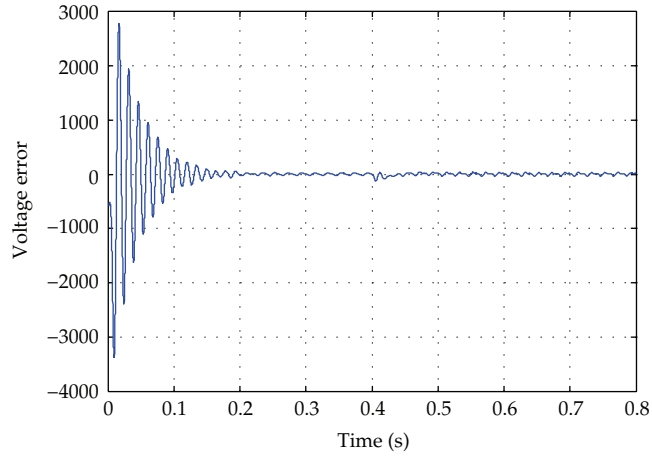

Figure 19: Voltage error between model reference voltage item and APF DC voltage.

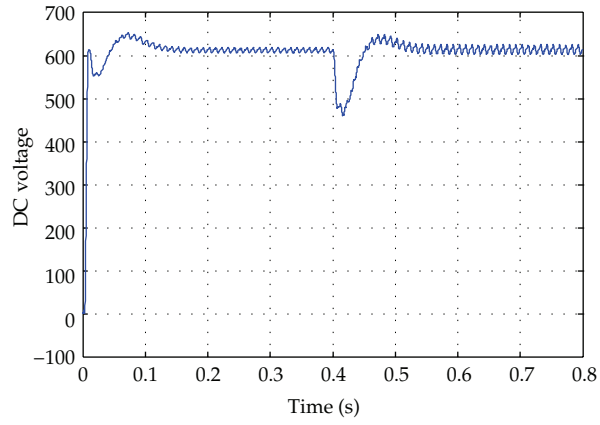

Figure 20: APF DC voltage using adaptive control.

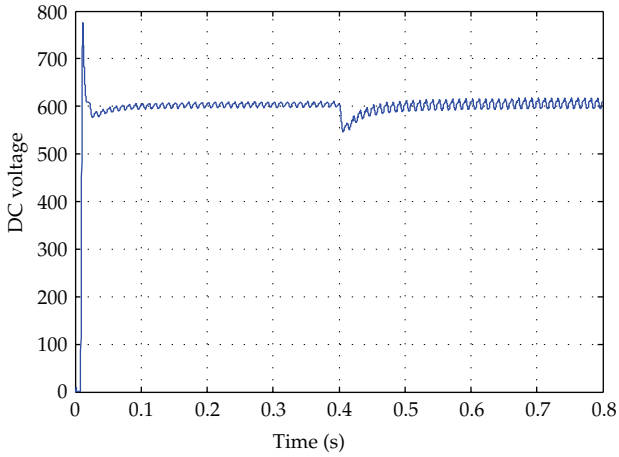

Figure 21: APF DC voltage using adaptive sliding mode control.

satisfactory adaptive and robust ability in the presence of the changing disturbances and nonlinear loads.

Acknowledgments

The authors thank the anonymous reviewer for useful comments that improved the quality of the paper. This work is partially supported by National Science Foundation of China under Grant no. 61074056, Natural Science Foundation of Jiangsu Province under Grant no. BK2010201, Scientific Research Foundation of High-Level Innovation, and Entrepreneurship Plan of Jiangsu Province. They also would like to thank the Fundamental Research Funds for the Central Universities under Grant no. 2012B06714.

References

[1] S. Rahmani, N. Mendalek, and K. Al-Haddad, "Experimental design of a nonlinear control technique for three-phase shunt active power filter," *IEEE Transactions on Industrial Electronics*, vol. 57, no. 103364, p. 3375, 2010.

[2] G. K. Singh, A. K. Singh, and R. Mitra, "A simple fuzzy logic based robust active power filter for harmonics minimization under random load variation," *Electric Power Systems Research*, vol. 77, no. 8, pp. 1101–1111, 2007.

[3] C. N. Bhende, S. Mishra, and S. K. Jain, "TS-fuzzy-controlled active power filter for load compensation," *IEEE Transactions on Power Delivery*, vol. 21, no. 3, pp. 1459–1465, 2006.

[4] M. I. M. Montero, E. R. Cadaval, and F. B. González, "Comparison of control strategies for shunt active power filters in three-phase four-wire systems," *IEEE Transactions on Power Electronics*, vol. 22, no. 1, pp. 229–236, 2007.

[5] J. Matas, L. Garcia de Vicuna, J. Miret, J. M. Guerrero, and M. Castilla, "Feedback linearization of a single-phase active power filter via sliding mode control," *IEEE Transactions on Power Electronics*, vol. 23, no. 1, pp. 116–125, 2008.

[6] C. C. Hua, C. H. Li, and C. S. Lee, "Control analysis of an active power filter using Lyapunov candidate," *IET Power Electronics*, vol. 2, no. 4, pp. 325–334, 2009.

[7] H. Komucugil and O. Kukrer, "A new control strategy for single-phase shunt active power filters using a Lyapunov function," *IEEE Transactions on Industrial Electronics*, vol. 53, no. 1, pp. 305–312, 2006.

[8] G. W. Chang and T. C. Shee, "A novel reference compensation current strategy for shunt active power filter control," *IEEE Transactions on Power Delivery*, vol. 19, no. 4, pp. 1751–1758, 2004.
[9] R. R. Pereira, C. H. Da Silva, L. E. B. Da Silva, G. Lambert-Torres, and J. O. P. Pinto, "New strategies for application of adaptive filters in active power filters," *IEEE Transactions on Industry Applications*, vol. 47, no. 3, pp. 1136–1141, 2011.
[10] L. Marconi, F. Ronchi, and A. Tilli, "Robust nonlinear control of shunt active filters for harmonic current compensation," *Automatica*, vol. 43, no. 2, pp. 252–263, 2007.
[11] L. Asiminoaei, F. Blaabjerg, S. Hansen, and P. Thøgersen, "Adaptive compensation of reactive power with shunt active power filters," *IEEE Transactions on Industry Applications*, vol. 44, no. 3, pp. 867–877, 2008.
[12] A. Luo, Z. Shuai, W. Zhu, R. Fan, and C. Tu, "Development of hybrid active power filter based on the adaptive fuzzy dividing frequency-control method," *IEEE Transactions on Power Delivery*, vol. 24, no. 1, pp. 424–432, 2009.
[13] D. Ribeiro, R. Azevedo, and C. Sousa, "A robust adaptive control strategy of active power filters for power-factor correction, harmonic compensation, and balancing of nonlinear loads," *IEEE Transactions on Power Electronics*, vol. 27, no. 2, pp. 718–730, 2012.
[14] A. A. Valdez, G. Escobar, and R. Ortega, "An adaptive controller for the shunt active filter considering a dynamic load and the line impedance," *IEEE Transactions on Control Systems Technology*, vol. 17, no. 2, pp. 458–464, 2009.
[15] K. K. Shyu, M. J. Yang, Y. M. Chen, and Y. F. Lin, "Model reference adaptive control design for a shunt active-power-filter system," *IEEE Transactions on Industrial Electronics*, vol. 55, no. 1, pp. 97–106, 2008.
[16] H. L. Jou, J. C. Wu, Y. J. Chang, and Y. T. Feng, "A novel active power filter for harmonic suppression," *IEEE Transactions on Power Delivery*, vol. 20, no. 2, pp. 1507–1513, 2005.
[17] H. A. Ramos-Carranza, A. Medina, and G. W. Chang, "Real-time shunt active power filter compensation," *IEEE Transactions on Power Delivery*, vol. 23, no. 4, pp. 2623–2625, 2008.
[18] P. A. Ioannou and J. Sun, *Robust Adaptive Control*, Prentice Hall, Englewood Cliffs, NJ, USA, 1995.